13th International Symposium on Turbulence and Shear Flow Phenomena (TSFP13)
Montreal, Canada, June 25-28, 2024

# STUDY OF CRESCENT WINGS IN BACKWARD AND FORWARD CONFIGURATIONS

**M. G. Mungal**
Mechanical Engineering Department
Santa Clara University
Santa Clara, CA USA
mgmungal@scu.edu

**Andrew K. Mahler**
Mechanical Engineering Department
Santa Clara University
Santa Clara, CA USA
amahler@scu.edu

## ABSTRACT

CFD investigations of generalized crescent wing shapes are performed using ANSYS-Fluent on low aspect ratio NACA 0012 wings up to an angle of attack of 60°. For straight and backward facing crescent wings, results show the "classical stall" behavior with sudden first stall at around 12-20° angle of attack, followed by lift recovery and a second stall at about 45° AoA. For forward facing crescent wings we observe a different type of "rolling stall" behavior characterized by a decreasing of the first stall but with a similar second stall. These findings are attributed to the different flow separation behaviors of the wings with back crescents showing separation initially at the tip region and growing quickly inboard with increasing AoA, while the forward crescent separates first at the inboard region and grows slowly outboard with AoA. Flow visualizations reveal corresponding significant differences in vortex patterns over the wing surface and in the wake region.

## INTRODUCTION

After previous investigation by Mungal & Benner (2022) into the forward fin motivated by certain tropical fish, and finding an experimental dataset by Ardonceau (1994) on backward swept crescent wings, we performed a comprehensive investigation into the forward and backward crescent wing shape by generalizing the formulation of Ardonceau. In addition, four models, one straight and three backward wings were tested by Ardonceau in a wind tunnel. While keeping these four, the wing planforms were also swept forward to new shapes by modifying his formulation for the ¼ chord position, while keeping the chord length the same. An essential difference is that straight and backward swept wings have a leading edge that is *convex* to the incoming flow, while the forward swept wing's leading edge is *concave* to the incoming flow. Since the vorticity is introduced through the no-slip condition at the leading edge, the vorticity distribution over the wing is different in forward *vs*. backward swept wings at the same angle of attack (AoA).

Earlier work on straight and backward crescent wings was pioneered by van Dam (1987) and van Dam et al. (1991) which suggested modest aerodynamic improvements for backward-facing wings, when compared to unswept elliptical wings. In the present study the airfoil is a NACA 0012, tapered towards the tip with a moderate aspect ratio of 5 (full wing) and a Reynolds number of approximately 500,000. Using SolidWorks, we replicated Ardonceau's wings, but some details of the experimental wing tip region are not available so we slightly truncated the wing in the tip region while adding some fillets to the model to imitate a practical model wing.

After modeling in SolidWorks, the crescent wing (half wing) was exported into ANSYS Workbench where Fluent was used to simulate the flow. We computed half of the experimental wind tunnel size by using a box size of 1.5 m (axial) x 1 m (height) x 0.6 m (span) with a flow speed of 56 m/s and base chord of 15.3 cm to match the Reynolds number. Owing to its accuracy in turbulent problems involving flow separations, the SST k-Omega turbulence model was used on a mesh with approximately 1.2 million cells including inflation layers along the wing surface and wake refinement as seen in Fig 1.

A notable difference in the simulations is that a symmetry condition is used at the wing root, while the experiment used an entire wing in the wind tunnel, i.e. twice as large as the simulations. Using the results of Ardonceau's wind tunnel experiments both the model and the simulation criteria were thus calibrated. We investigated a total of seven configurations, Fig. 2, consisting of three backward swept, one straight and three forward swept wings. The straight case is essentially an elliptical wing. The three backward sweeps, together with the straight wing simulate Ardonceau's experiments.

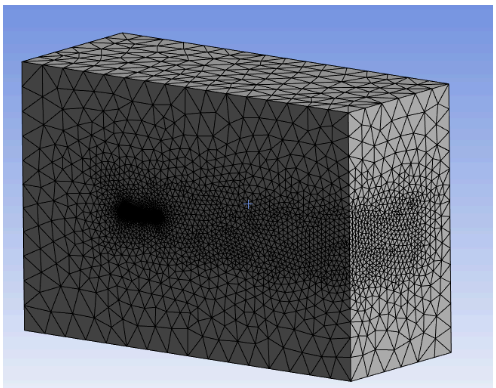

Figure 1. Computational domain used in this study showing grid refinements. Uniform flow inlet on left; constant pressure outlet at right, symmetry mirror plane at front, three slip boundaries at top, bottom, and back.

## RESULTS AND DISCUSSION

Two preliminary cases were used to establish the fidelity of the CFD code. We found that Fluent was better able to capture Ardonceau's data up to and including first stall when compared to Star-CCM+. In addition, a two-dimensional simulation of a NACA 0012 airfoil at Re = 500,000 in a box of 50 x 50 chords was performed with both CFD codes. Fluent produced the results shown in Fig. 3, in good agreement with experimental studies of Critzos et al. (1955) and Sheldahl & Klimas (1981). The lift coefficient is seen to increase linearly at low AoA until it experiences a sudden decrease in lift over an angle of attack range of 12°- 20° (this decreasing region will be called First Stall, S1). After stalling the lift recovers (this region will be called Recovery, R1) while reaching a second peak of similar magnitude at around 45° AoA. Then the lift gradually decreases again (this region will be called Second Stall, S2) towards a slightly positive value at 90° AoA. Past 90° the sharp edge of the airfoil becomes the leading edge and a similar lift behavior is seen from 90° to 180° AoA although at somewhat reduced magnitudes. All subsequent results were performed using Fluent.

Moving to crescent wings, changing how much and in which direction the wing was curved directly affected its stalling behavior. Figure 4 shows the Lift and Drag Coefficients, CL, CD for all seven configurations vs. AoA. The values generally agree with Ardonceau's experimental results (limited to 0°- 16° AoA) up through first stall. His peak values are somewhat higher but the relative trends of higher peak values at higher stall AoA for more backward sweep is well captured. Furthermore, the experimental wing model may experience instantaneous asymmetry whereas the simulation is constrained to be symmetrical, as noted previously. These lift results show that the straight and backward crescent wings display the classical two-stall behavior seen in experimental studies of two-dimensional wings which extend to high AoA (Critzos et al., 1955; Sheldahl & Klimas, 1981).

The forward crescents however showed a different behavior which we designate as a "Rolling Stall." As the wing's leading edge curved more and more into the oncoming flow, the S1 region becomes smaller because both the lift peak is lower and the R1 region generally increases. Eventually the S1 region disappears for the most forward case, i.e. that there is no sudden loss of lift, but only a gradual increase until the S2 region. We note that Mungal & Benner (2022) observed the "rolling stall" behavior experimentally at AoA up to 30°, the maximum angle for which they tested.

Drag Coefficients are also shown in Fig. 4 where the backward crescents generally displayed lower drag at higher AoA while the forward crescents had less drag in the S1 region (12°-20°). For all models it is important to note that in the S1 region, the reported values are averages because the simulation results would oscillate as the flow continuously separates and re-attaches. These results for the forward cases are clearly different and the flow visualizations shown next will reveal some key reasons on why this unique behavior is present.

Figure 5 is a side-by-side comparison of the full backward, straight and full forward configurations at AoA of 8° (i.e. in the linear pre-stall region). The upper portion of the figure shows streamlines which are offset about 1/100 of a chord above a white wing surface to highlight the flow development over the wing and into the wake region. Note that the streamlines are color coded to show the magnitude of the flow velocity, so red is expected at the leading edge of the wing as the flow accelerates, and blue towards the training edge as the flow decelerates. In addition, the figure also shows a wall shear stress wing surface map displaced to the right. The displacement is necessary to allow the streamlines and wall shear to be compared directly, side-by-side, without color interference of the two if they were overlaid onto the same wing. The wall shear is expected to be higher (red) towards the leading edge and lower (blue) towards the trailing edge of the wing, based on the local flow speed.

The lower portion of the figure shows the curl of velocity in the x-direction using a volume rendering approach. Mahler (2024) describes the many choices of variables available in post processing to visualize the flow (e.g. helicity, Lambda 2, Q invariant, etc.), and curl-x is used here as it shows the evolution of the streamwise vorticity from the leading edge of the wing into the downstream wake. Each figure caption also shows CL for each image from left to right so the lift and corresponding flow images can be compared. These visualizations are used to highlight some of the most important differences between these three geometries and how they impact the flow. Figures 6-8 show similar plots at AoA of 14° (the S1 first stall region), 30° (the R1 recovery region) and 60° (the S2 deep stall region).

Beginning with Fig. 5 at 8° AoA the streamlines indicate the flow is fully attached for each case, as expected. The wall shear varies from high values (red) at the leading edge to low values (blue) at the trailing edge. The curl-x volume renderings highlight subtle differences in streamwise (axial) vorticity in the three cases, which would not be obvious from examination of only the velocity streamlines. We note that positive axial vorticity, similar to the tip vortex, is seen over the surface of the backward wing, while surprisingly, negative (i.e. blue) vorticity exists over the surface of the forward crescent wing. This difference is believed to be a result of the concave *vs*. convex leading edge shape and its impact on the vorticity formation and distribution over the wing surface. The straight wing shows a behavior which lies between that of the forward and backward crescents, but closer in nature to the backward crescent.

Figure 6 in the S1 region at 14° AoA shows details of the separation process for the three wings. The wall shear is now more complex when compared to 8° AoA and the streamlines indicate the separation regions which are primarily outboard for the backward crescent, inboard for the forward crescent, and nominally two-dimensional for the straight case. For the back crescent, the tip region of the wing is where the flow first begins to separate. This is evidenced by the vortical flow near the tip, low (blue) velocities, and the low wall shear stresses seen on the wing surface. On the other hand, the forward crescent begins separation at the inboard region of the wing. Again this is seen in the low shear stress values and the low velocities. Note that in general, the forward crescent needed an expanded range for the wall shear stress legend to accurately show its details. Knowing this, the tip of the forward crescent maintains a very strong wall shear stress level. We also note that zero wall shear stress is indicative of the surface separation lines seen in experiments and those observed here often show the complexity seen in van Dam et al. (1991).

Another important feature of this flow is seen in curl-x i.e. the streamwise vorticity. This measure was chosen as it best captures the uniqueness of the flow allowing a view of both magnitude, and more importantly, direction of the flow. As seen in Fig. 6 the back crescent creates a positive curl in the x-direction combining the positive tip curl with the curl generated in the separation. The forward crescent on the other hand generates a negative curl from the separation. This creates three distinct cores for the vorticity rather than the backward crescent that combines into one. Significant regions of negative vorticity (blue curl-x) appear on the forward crescent, which is not observed for the backward crescent. It is also interesting that both the straight and backward wings have the same lift coefficient, but very different wake vorticity distributions.

The simulations generally show that as the forward wing increases its AoA the high shear tip region shrinks as the separation region expands slowly outwards across the wing surface. This slowly growing separation region likely explains why this wing has eliminated the S1 region. On the other hand, the back crescent quickly expands its separation region, going from no separation to complete separation in about a 6° AoA range, thus displaying the classical sudden-stall behavior.

Figure 7 at 30° AoA in the R1 region shows full-blown separation bubbles across the backward and straight crescents (as indicated by the blue recirculating streamlines), but only an inboard separation for the forward crescent with the tip region showing attached flow (green streamlines). This is consistent with the forward crescent now having the highest lift coefficient of the three wings at 30° AoA. The vorticity of the forward crescent is seen to consist of three primary cores, unlike the backward case which shows a single core. The straight case shows elements of both crescents. At this higher AoA more vorticity is shed from the trailing edge region of the wing leading to the positive curl-x seen downstream. This behavior is only moderately seen in the forward crescent, positioned adjacent to the negative curl-x, but becomes more prominent at higher AoA.

Finally, Fig. 8 at 60° AoA in the deep stall S2 region shows similar wall shear for all cases (light blue), but very different separation bubble formation for each case. The backward crescent shows a dominant recirculation bubble across the entire wing, while the straight and forward crescent shows upper and lower bubbles of differing sizes and orientations. All wings now have the same lift coefficient, yet quite different axial vorticity distributions in the wake regions. Furthermore, the vorticity is seen to be primarily shed from the leading and trailing edges of each wing under these deep stall conditions.

When interpreting the results of Figs. 5-8, it is again useful to remember that vorticity is first introduced into the flow at the leading edge of the wing so the spatial layout of the leading edge plays an important role. Additionally, vorticity undergoes tilting and stretching mechanisms and primarily the x-component has been shown here. Figure 9 shows the three components curl-y, curl-z and curl-x for the full backward and full forward crescent wings at 20° AoA, in addition to other vortical measures described by Mahler (2024). It is clear that curl-x provides the most comprehensive picture of the flow and the wake vortex development, hence its usage here.

Finally, it is perhaps worth noting that some larger birds (e.g. owls, eagles) deliberately move their wings into the forward configuration when landing or catching prey close to the ground. While wing flapping is important, our results suggest that forward wing positioning would be beneficial for at least two reasons when compared with wings kept in a nominally straight position. First, sudden stall is eliminated so the bird can exercise a large range of angles of attack, from low to high, without any sudden loss of lift as the wings are pitched upwards. Secondly, moving the wings to the forward configuration means that the center of lift will also move forward allowing the bird to swing its body weight and legs forward in a gravitationally stable manner suitable for catching prey, or for landing. In all cases, drag is increased, and this may actually be beneficial for the maneuver.

## CONCLUSIONS

This computational study, rooted in the prior research and wind tunnel tests of Ardonceau (1994) investigates the unique flow of crescent wings when extended to forward crescent shapes. While backward crescents display a classical two-stall behavior, the forward crescent instead shows a “rolling stall” behavior mainly by elimination of the sudden first stall. These lift behaviors are seen to be caused by the different flow separations across the wing surface. For the backward crescent, separation starts at the tip region of the wing, then quickly expands across the entire wing at first stall. On the other hand for the forward crescent, separation begins at the root section of the wing, gradually expanding outwards across the wing with a strong tip vortex and some attached flow. The straight elliptical wing is an intermediary but closer in behavior to the backward crescent. These results suggest the importance of the leading edge shape, concave or convex to the incoming flow, and its effect upon the lift, drag and the resulting vorticity distribution of the wing.

## ACKNOWLEDGEMENTS

This work was supported by an internal grant from Santa Clara University. We thank Jason Chong from the Engineering Computing Center for software support.

## REFERENCES

Ardonceau P. L., 1994, “Aerodynamic Properties of Crescent Wing Planforms” *J. Aircraft*, 31 (5): 462-465.

Critzos, C. C., Heyson, H. H. & Boswinkle Jr., R. W., Jan. 1955, “Aerodynamic Characteristics of NACA0012 Airfoil Section At Angles of Attack From 0° To 180°” *NACA Technical Note 3361*.

Mahler, A. K., 2024, “Comparison of CFD Visualization Methods for Separated Flows” *AIAA 2024 Region VI Student Conference*, 23-24 March 2024, Santa Clara University, Santa Clara, CA.

Mungal, M. G. & Benner, T., 2022, “The Forward-Facing Fin - An Unusual Hydrodynamic Design” *Twelfth International Symposium on Turbulence and Shear Flow Phenomena (TSFP12)*, Osaka, Japan, July 19-22, 2022.

Sheldahl, R. E. & Klimas, P. C., March 1981, “Aerodynamic Characteristics of Seven Symmetrical Airfoil Sections Through 180-Degree Angle of Attack for Use in Aerodynamic Analysis of Vertical Axis Wind Turbines” *Sandia Report SAND80-2114*.

Van Dam, C. P., 1987, “Induced-Drag Characteristics of Crescent-Moon-Shaped Wings,” *J. Aircraft*, 24 (2), 115-119.

Van Dam, C. P., Vigjen, P. M. H. W. & Holmes, B. J., 1991, “Aerodynamic Characteristics of Crescent and Elliptic Wings at High Angles of Attack” *J. Aircraft* 28 (4): 253-260.

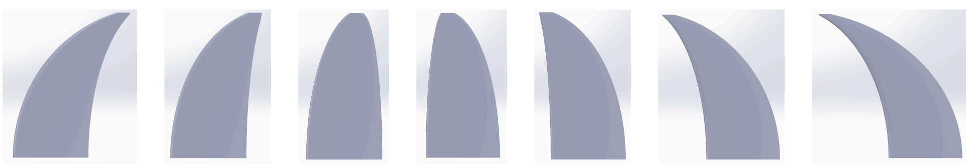

Figure 2 - Planform of the seven shapes investigated for flow from left to right. Leftmost: full back. Center: Straight. Rightmost: Full Forward

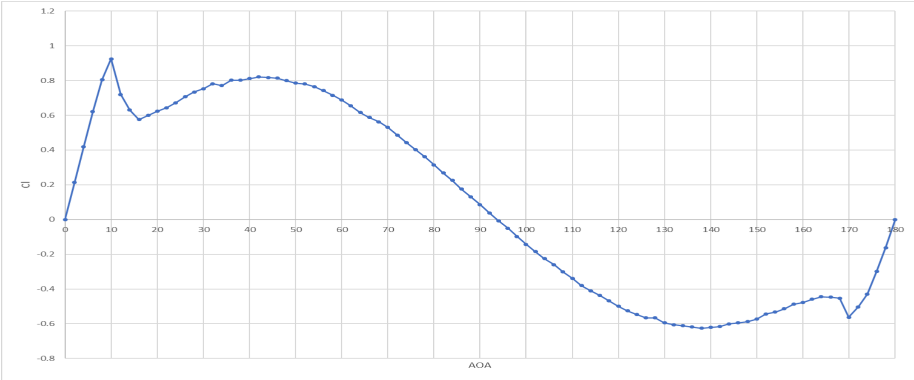


Figure 3- Lift Coefficient vs AoA of NACA 0012 two-dimensional airfoil at Re=500,000 using Fluent.

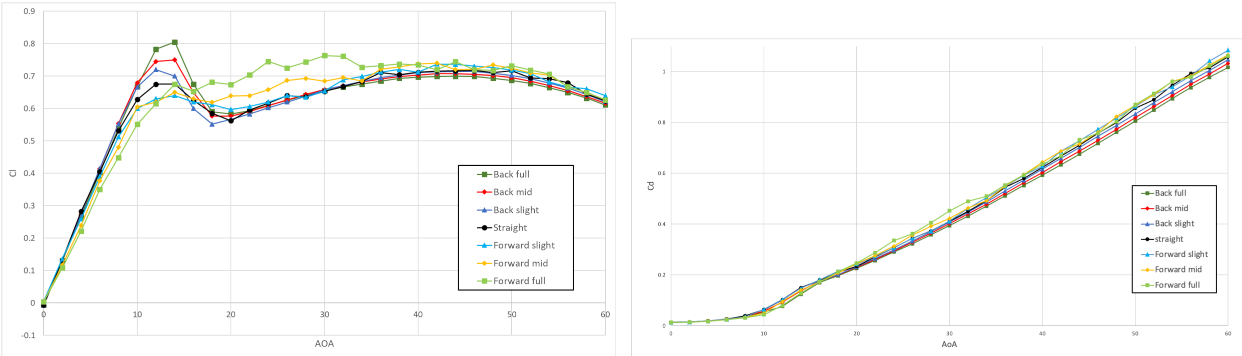


Figure 4: Lift and Drag Coefficients vs Angle of Attack

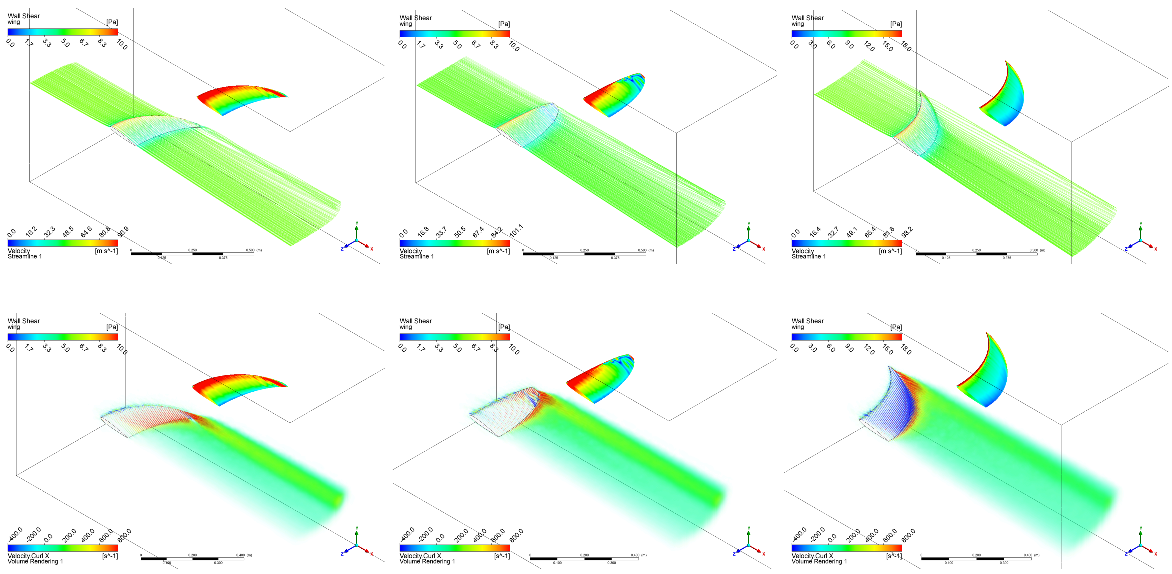

Figure 5: Comparison of: Left - full back, Center - straight and Right - full forward crescent wing at AoA 8°. CL= 0.67, 0.63, 0.55 from left to right. Top: streamlines. Bottom: curl-x. Displaced wall shear stress also shown.

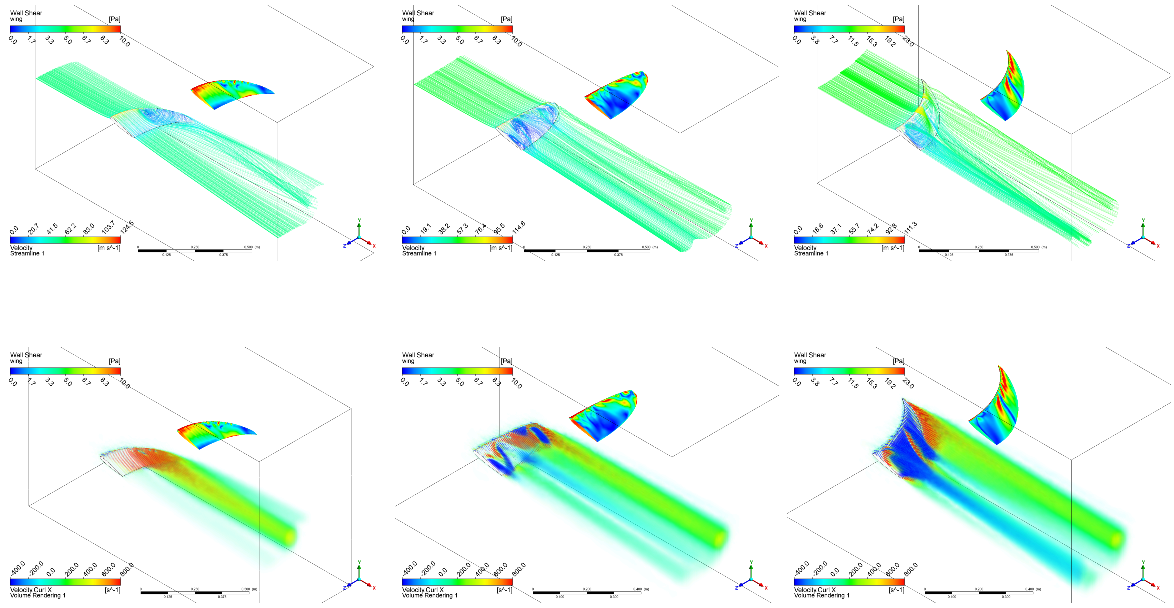

Figure 6: Comparison of: Left - full back, Center - straight and Right - full forward crescent wing at AoA 14°. CL= 0.80, 0.68, 0.68 from left to right. Top: streamlines. Bottom: curl-x. Displaced wall shear stress also shown.

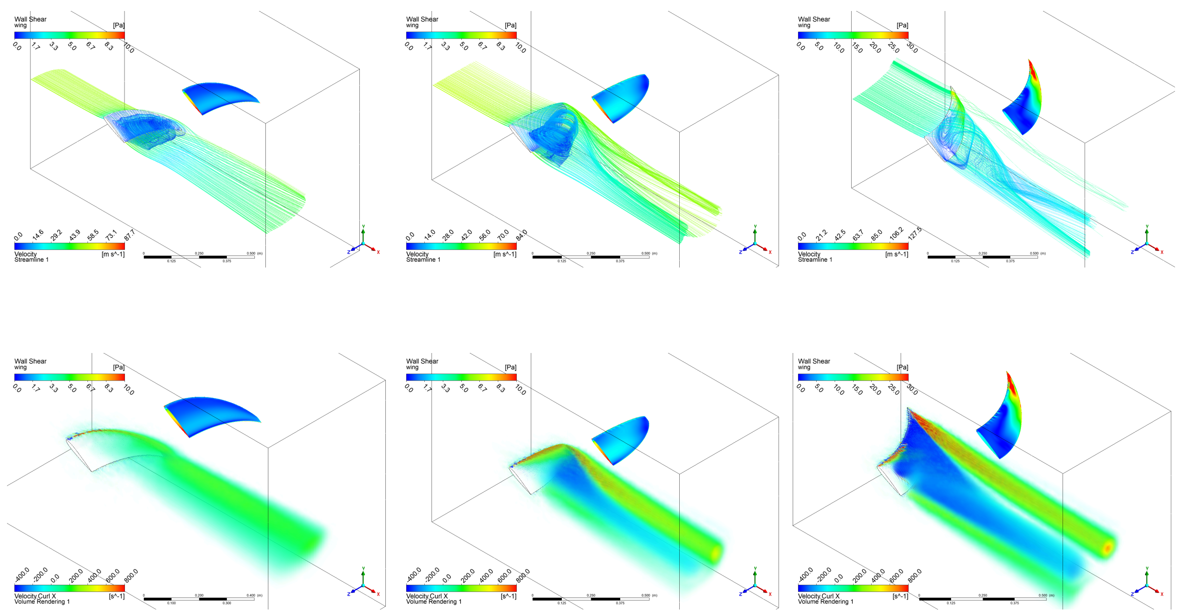

Figure 7: Comparison of: Left - full back, Center - straight and Right - full forward crescent wing at AoA 30°. CL= 0.65, 0.65, 0.76 from left to right. Top: streamlines. Bottom:curl-x. Displaced wall shear stress also shown.

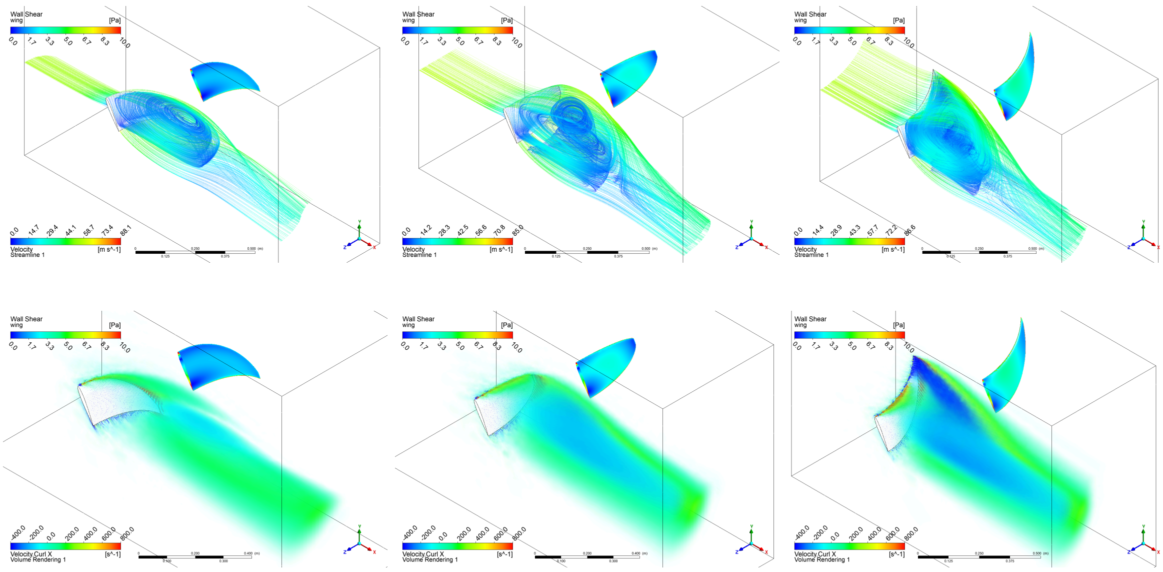

Figure 8: Comparison of: Left - full back, Center - straight and Right - full forward crescent wing at AoA 60°. CL= 0.62, 0.62, 0.63 from left to right. Top: streamlines. Bottom: curl-x. Displaced wall shear stress also shown.

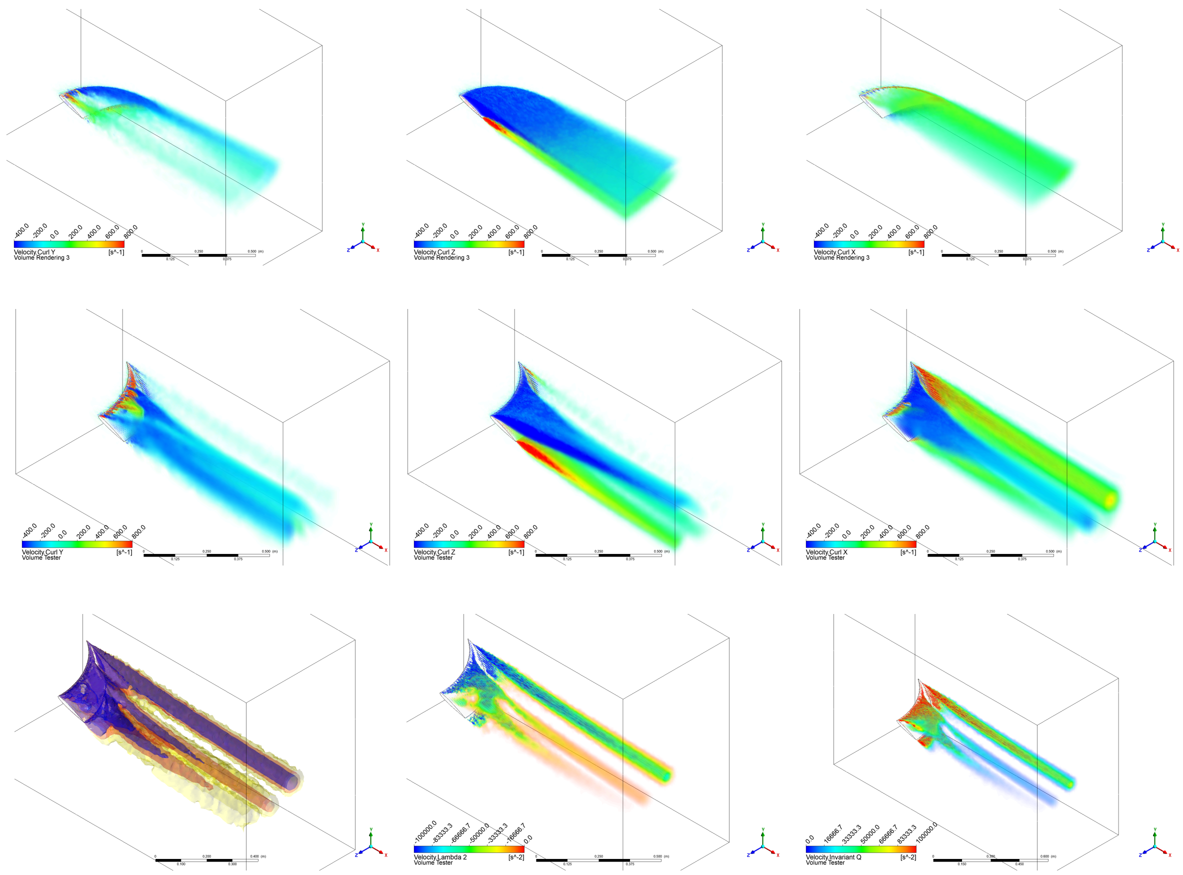

Figure 9: Comparison of curl-y, curl-z, curl-x at AoA 20°. Top Row - full backward crescent wing, Middle Row - full forward crescent wing. Bottom Row - full forward crescent showing Swirling Strength iso-surfaces, Lambda 2, Invariant Q, from left to right.